

Reassessing the SIGW Interpretation of PTA Signal: The Role of Third-Order Gravitational Waves and Implications for the PBH Overproduction

Zhi-Chao Zhao,¹ Sai Wang,^{2,*} Qing-Hua Zhu,³ and Xin Zhang^{4,5,6}

¹*Department of Applied Physics, College of Science, China Agricultural University,
17 Qinghua East Road, Haidian District, Beijing 100083, China*

²*School of Physics, Hangzhou Normal University,
No.2318 Yuhangtang Road, Yuhang District, Hangzhou 311121, China*

³*School of Physics, Chongqing University, Chongqing 401331, China*

⁴*Liaoning Key Laboratory of Cosmology and Astrophysics,
College of Sciences, Northeastern University, Shenyang 110819, China*

⁵*National Frontiers Science Center for Industrial Intelligence and Systems Optimization,
Northeastern University, Shenyang 110819, China*

⁶*MOE Key Laboratory of Data Analytics and Optimization for Smart Industry,
Northeastern University, Shenyang 110819, China*

In light of recent interpretations attributing pulsar timing array (PTA) signal to second-order gravitational waves induced by linear cosmological curvature perturbations in the early universe, the overproduction of primordial black holes (PBHs) poses a theoretical tension. In this work, we address this issue through extending such a scalar-induced gravitational wave (SIGW) framework to include third-order gravitational waves, which allow for a substantial enhancement in the spectral amplitude of SIGWs. Analyzing a combined dataset from cosmic microwave background and baryon acoustic oscillations, we derive cosmological constraints on the physical energy-density fraction of cosmological gravitational waves. Further incorporating PTA data, we obtain constraints on the spectral amplitude and peak frequency of SIGWs. Our results indicate that the parameter region favored by the data combination can to some extent alleviate the PBH overproduction problem, thereby supporting the theoretical consistency of our model. Furthermore, we demonstrate the robustness of our SIGW interpretation for the PTA signal by extending the analysis to include a gravitational wave background from supermassive black hole binaries. These findings are poised for further scrutiny with future high-precision observations.

I. INTRODUCTION

Evidence for a nanohertz gravitational-wave background (GWB) has recently been reported with high significance by multiple pulsar timing arrays (PTAs), with the inferred signal consistent with the expected spatial correlations of an isotropic background [1–4]. While an astrophysical origin from supermassive black hole binaries (BHBs) remains a well-motivated explanation, the PTA band is also sensitive to early-Universe mechanisms that generate gravitational radiation long before recombination [5–8]. Establishing or ruling out a cosmological origin is therefore of broad interest. It would open a window onto primordial physics at scales far smaller than those directly probed by the cosmic microwave background (CMB). For recent broad reviews on cosmological stochastic gravitational-wave backgrounds and source classes (e.g., see Ref. [9]).

* Contact author; wangsai@hznu.edu.cn

Among cosmological interpretations, the scalar-induced gravitational waves (SIGWs) provide a particularly predictive framework. In this scenario, enhanced primordial linear curvature perturbations on small scales source tensor perturbations at nonlinear order when the corresponding modes reenter the horizon, yielding a stochastic background whose spectrum is calculable once the small-scale curvature power spectrum, denoted as $\mathcal{P}_\zeta(k)$, is specified [10–15]. A central feature of the SIGW framework is that the same enhancement of curvature perturbations that boosts the tensor perturbations generically also triggers the formation of primordial black holes (PBHs) (e.g., see reviews in Ref. [16]). As a result, SIGWs and PBHs are tightly linked probes of the small-scale curvature sector, with the PTA-sensitive frequencies mapping to PBH masses in the sub-solar regime in many benchmark setups.

This tight connection immediately leads to the PBH overproduction problem [7]. In the standard Gaussian treatment, fitting a PTA-level SIGW signal with the conventional second-order induced spectrum typically requires an enhancement of the small-scale curvature power to the order of $\mathcal{O}(10^{-2}\text{--}10^{-1})$. However, PBH formation depends exponentially on the variance and, more generally, on the tail of the coarse-grained curvature distribution. Consequently, parameter values that reproduce the PTA signal can predict PBH abundances that overshoot observational bounds by several orders of magnitude, rendering a purely Gaussian second-order gravitational-wave interpretation strongly constrained or disfavored quantitatively. A substantial literature has explored ways to relieve this tension while maintaining a cosmological origin, including engineered primordial non-Gaussianity, nonstandard early-time expansion histories, and additional model-building ingredients that alter the mapping between $\mathcal{P}_\zeta(k)$, SIGWs, and PBHs [7, 17–46].

In this context, it is crucial to revisit a theoretical assumption that is often implicit in phenomenological analyses: that the induced background is adequately described by the second-order contribution alone. When the curvature enhancement is sizable, precisely the regime suggested by PTA fits, higher-order contributions to the induced tensor sector can become non-negligible [37]. Recent computations indicate that third-order SIGWs can contribute comparably to, or even dominate, the integrated energy density for sufficiently large peak amplitudes, thereby modifying the relation between the inferred curvature power spectrum and the associated PBH abundance [37, 47–51]. Because PBH abundances respond exponentially to the required curvature amplitude whereas the SIGW spectrum responds more mildly, any mechanism that increases the gravitational-wave yield at fixed \mathcal{P}_ζ , including higher-order gravitational-wave contributions, has the potential to alleviate overproduction by lowering the curvature amplitude needed to match the PTA signal.

A complementary ingredient is the use of external cosmological information. Independent constraints on the total energy density of cosmological gravitational waves from the CMB anisotropies and baryon acoustic oscillations (BAO) measurements provide an essentially model-agnostic bound on the SIGW energy-density fraction spectrum across frequencies above $\sim 10^{-15}$ Hz, and thus act as a late-time anchor for any early-Universe explanation of the PTA signal [52–57]. Moreover, in practice, SIGW fits to the PTA band may probe only the infrared (IR) tail of the SIGW spectrum for peaked curvature power spectra, which can lead to degeneracies between the peak amplitude and peak scale when PTA data are used alone. Cosmological bounds on the total gravitational-wave energy density therefore play a key role in pinning down the underlying small-scale curvature parameters in a way that is consistent across cosmic epochs. This complementarity has been

emphasized in recent joint CMB, BAO, and PTA analyses of cosmological gravitational-wave scenarios [37–41, 58–63].

Motivated by the considerations above, we perform a unified Bayesian study of the SIGW interpretation of the nanohertz PTA signal in a framework that treats SIGWs consistently up to third order. For definiteness and transparency, we parameterize the small-scale curvature sector with a sharply peaked primordial spectrum characterized by an amplitude A_ζ and a characteristic scale (equivalently, a peak frequency f_*), and compute the resulting present-day SIGWs including both second- and third-order contributions. We first derive constraints on the integrated energy-density fraction of cosmological gravitational waves from a joint analysis of CMB and BAO data [56, 64–68], and then incorporate PTA information, focusing on the North American Nanohertz Observatory for Gravitational Waves 15-year (NANOGrav 15yr) data release [1], to constrain the SIGW spectrum parameters. We further test robustness by extending the inference to include an additional GWB component from BHBs. Within this combined framework, we identify regions of parameter space preferred by the data in which the PTA signal can be reproduced while the implied PBH abundance remains subdominant, thereby significantly alleviating the PBH overproduction tension in Gaussian SIGW scenarios. We also provide prospective forecasts for joint constraints that combine PTA data with next-generation CMB and BAO observations [69–72].

The remainder of the paper is organized as follows. In Sec. II, we summarize the SIGW formalism up to third order and define the gravitational-wave energy-density observables used in the analysis. In Sec. III, we present our Bayesian methodology and the joint constraints from CMB, BAO, and PTA datasets (with and without considering BHBs), and we report prospective joint constraints from PTA together with next-generation CMB and BAO mock data [69–72]. In Sec. IV, we translate the inferred curvature parameters into PBH abundances and discuss the implications for the overproduction problem. We conclude in Sec. V.

II. THEORETICAL PERSPECTIVE OF SIGWS

In this section, we briefly summarize the theoretical results of SIGWs that will be constrained with observational data in the next section.

A. Nonlinear cosmological perturbations

The energy-density fraction spectrum of SIGWs is a key physical quantity that connects primordial curvature perturbations with gravitational-wave observations [15]. In previous studies [10–15], this spectrum has typically been derived from second-order tensor perturbations, denoted as $h_{ij}^{(2)}$, which are generated by the quadratic coupling of linear cosmological scalar perturbations. However, when the amplitude of these perturbations is sufficiently large, it becomes theoretically necessary to account for tensor perturbations produced by higher-order couplings of these perturbations. The primary next-order correction leads to third-order tensor perturbations, denoted as $h_{ij}^{(3)}$, arising from the cubic couplings of these perturbations [37, 48]. In this study, we will employ a theoretical framework for SIGWs that incorporates both second- and third-order tensor perturbations, in order to analyze the latest PTA data and address the overproduction problem of

PBHs.

Specifically, the second- and third-order tensor perturbations are defined in the perturbed spatially-flat Friedmann-Robertson-Walker metric as [37, 48]

$$ds^2 = a^2(\eta) \left\{ - \left(1 + 2\phi^{(1)} + \phi^{(2)} \right) d\eta^2 + V_i^{(2)} d\eta dx^i + \left[\left(1 - 2\psi^{(1)} - \psi^{(2)} \right) \delta_{ij} + \frac{1}{2} h_{ij}^{(2)} + \frac{1}{6} h_{ij}^{(3)} \right] dx^i dx^j \right\}, \quad (1)$$

where the superscript (n) denotes perturbations of n -th order, $a(\eta)$ represents the scale factor of the universe at a conformal time η , ϕ and ψ stand for scalar perturbations, V_i denotes vector perturbations, and h_{ij} represents tensor perturbations. Here, all perturbations are calculated in the conformal Newtonian gauge [73]. In this work, we neglect the linear anisotropic stress, i.e., $\psi^{(1)} = \phi^{(1)}$. In the early universe after the end of inflation, the linear (comoving) curvature perturbations are given by [74]

$$\zeta = \frac{3}{2} \psi^{(1)} \Big|_{\eta=0}. \quad (2)$$

They are frozen on superhorizon scales, and begin to evolve after horizon reentering. The power spectrum of primordial linear curvature perturbations is defined by

$$\langle \zeta_{\mathbf{k}} \zeta_{\bar{\mathbf{k}}} \rangle = (2\pi)^3 \delta(\mathbf{k} + \bar{\mathbf{k}}) \mathcal{P}_\zeta(k), \quad (3)$$

where \mathbf{k} is the wavevector, and k is the wavenumber. In this study, we take $\mathcal{P}_\zeta(k)$ to be a monochromatic function of k , namely, [7, 15]

$$\mathcal{P}_\zeta(k) = A_\zeta k_* \delta(k - k_*), \quad (4)$$

where A_ζ is the spectral amplitude, and k_* is a characteristic wavenumber. Both A_ζ and k_* are independent parameters to be inferred in Section III.

The equations of evolution for the second- and third-order tensor perturbations are determined by Einstein's gravitational field equations. To be specific, they are given by [37]

$$h_{ij}^{(2)''} + 2\mathcal{H}h_{ij}^{(2)'} - \Delta h_{ij}^{(2)} = -4\Lambda_{ij}^{lm} \mathcal{S}_{lm}^{(2)}[\psi^{(1)}, \psi^{(1)}], \quad (5)$$

$$h_{ij}^{(3)''} + 2\mathcal{H}h_{ij}^{(3)'} - \Delta h_{ij}^{(3)} = -12\Lambda_{ij}^{lm} \left(\mathcal{S}_{lm}^{(3)}[\psi^{(1)}, \psi^{(1)}, \psi^{(1)}] + \mathcal{S}_{lm}^{(3)}[\psi^{(2)}[\psi^{(1)}, \psi^{(1)}], \psi^{(1)}] + \mathcal{S}_{lm}^{(3)}[\phi^{(2)}[\psi^{(1)}, \psi^{(1)}], \psi^{(1)}] + \mathcal{S}_{lm}^{(3)}[V^{(2)}[\psi^{(1)}, \psi^{(1)}], \psi^{(1)}] + \mathcal{S}_{lm}^{(3)}[h^{(2)}[\psi^{(1)}, \psi^{(1)}], \psi^{(1)}] \right), \quad (6)$$

where $\mathcal{H} = \mathcal{H}(\eta)$ is the conformal Hubble parameter, Δ is the Laplacian operator, Λ_{ij}^{lm} is the transverse-traceless projection operator, and $\mathcal{S}_{lm}^{(2)}$ and $\mathcal{S}_{lm}^{(3)}$, respectively, stand for the second- and third-order source terms. Here, we show that $h_{ij}^{(2)}$ is sourced by quadratic couplings of $\psi^{(1)}$ [14, 15], while $h_{ij}^{(3)}$ is sourced by cubic couplings of $\psi^{(1)}$ [37, 47, 48]. The second-order perturbations $\phi^{(2)}$, $\psi^{(2)}$, $V_i^{(2)}$, and $h_{ij}^{(2)}$ are also sourced by quadratic couplings of $\psi^{(1)}$, acting as intermediate sources for $h_{ij}^{(3)}$ [37, 48]. The explicit formulas for $\mathcal{S}_{lm}^{(2)}$ and $\mathcal{S}_{lm}^{(3)}$ are outlined in Ref. [37]. Here, we disregard

the dissipation effect due to neutrino diffusions when decoupling, since this effect is negligible to our study [75–77].

For the second- and third-order tensor perturbations, respectively, the power spectra are defined by their two-point correlations, i.e.,

$$\langle h_{ij,\mathbf{k}}^{(n)} h_{\bar{\mathbf{k}}}^{(n),ij} \rangle = 2(2\pi)^3 \delta(\mathbf{k} + \bar{\mathbf{k}}) \mathcal{P}_h^{(n)}(k, \eta), \quad (7)$$

where $n = 2, 3$ denotes the order of tensor perturbations, \mathbf{k} still denotes the wavevector, and k still denotes the wavenumber. Further combining with Eqs. (2,3,5,6), we get their formulas, i.e. [37, 48]

$$\mathcal{P}_h^{(2)} = \frac{k^3}{4\pi} \left(\frac{2}{3}\right)^4 \int \frac{d^3 p}{|\mathbf{k} - \mathbf{p}|^3 |\mathbf{p}|^3} \mathcal{P}_\zeta(|\mathbf{k} - \mathbf{p}|) \mathcal{P}_\zeta(p) \mathcal{K}^{(2)}(\mathbf{k}, \mathbf{p}, \eta), \quad (8)$$

$$\mathcal{P}_h^{(3)} = \frac{k^3}{32\pi^2} \left(\frac{2}{3}\right)^6 \int \frac{d^3 p d^3 q}{|\mathbf{k} - \mathbf{p}|^3 |\mathbf{p} - \mathbf{q}|^3 |\mathbf{q}|^3} \mathcal{P}_\zeta(|\mathbf{k} - \mathbf{p}|) \mathcal{P}_\zeta(|\mathbf{p} - \mathbf{q}|) \mathcal{P}_\zeta(q) \mathcal{K}^{(3)}(\mathbf{k}, \mathbf{p}, \mathbf{q}, \eta), \quad (9)$$

where $\mathcal{K}^{(2)}$ and $\mathcal{K}^{(3)}$, respectively, stand for kernels for the source terms $\mathcal{S}_{lm}^{(2)}$ and $\mathcal{S}_{lm}^{(3)}$, as outlined in Ref. [37]. Further considering Eqs. (4), we get

$$\mathcal{P}_h^{(2)} \propto A_\zeta^2, \quad (10)$$

$$\mathcal{P}_h^{(3)} \propto A_\zeta^3, \quad (11)$$

which indicates that, compared with the second-order tensor perturbations, the third-order tensor perturbations are expected to be subdominant when A_ζ is smaller than a critical value, and vice versa.

B. SIGW energy-density fraction spectrum

Let us introduce one of the most important observables. Incorporating both the second- and third-order tensor perturbations, the energy-density fraction spectrum during the epoch of radiation domination is given as [37]¹

$$\Omega_{\text{GW}}(k, \eta) = \frac{1}{24} \left(\frac{k}{\mathcal{H}}\right)^2 \left(\mathcal{P}_h^{(2)}(k, \eta) + \frac{1}{9} \mathcal{P}_h^{(3)}(k, \eta) \right), \quad (12)$$

where $\mathcal{P}_h^{(2)}$ and $\mathcal{P}_h^{(3)}$, respectively, are given by Eq. (8) and Eq. (9). As the observable, the present-day energy-density fraction spectrum of SIGWs is given by [78]

$$\Omega_{\text{GW},0}(k) = \Omega_{r,0} \left(\frac{g_{*,\rho}(T)}{g_{*,\rho}(T_{\text{eq}})} \right) \left(\frac{g_{*,s}(T_{\text{eq}})}{g_{*,s}(T)} \right)^{\frac{4}{3}} \Omega_{\text{GW}}(k, \eta), \quad (13)$$

where $\Omega_{r,0} \simeq 4.2 \times 10^{-5} h^{-2}$ is the present-day energy-density fraction of radiation [79], h is the dimensionless Hubble constant, and both $g_{*,\rho}(T)$ and $g_{*,s}(T)$ are the effective numbers of relativistic degrees of freedom at the cosmic temperature T [80]. The subscript _{eq} denotes quantities at the

¹ This formula is not the same as that of Ref. [37], as there are typos in the latter.

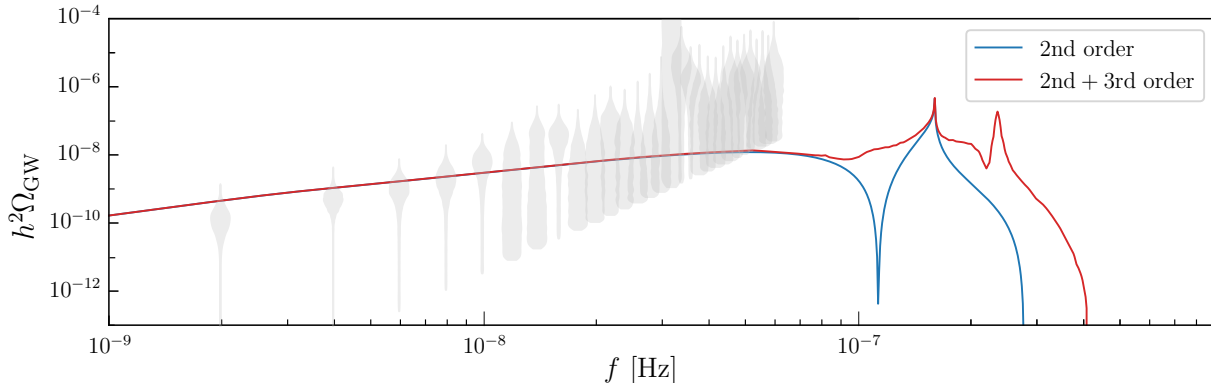


FIG. 1. Illustrative figure for the SIGW energy-density fraction spectra. The blue solid curve shows the contribution from second-order components only, while the red solid curve includes both second- and third-order components. Both spectra are computed using the same parameter set (A_ζ, f_*) , corresponding to the median values in the joint PTA, CMB, and BAO constraints on the SIGW spectrum (i.e., the first row of Tab. I). The grey violins represent the NANOGrav 15yr dataset [7].

epoch of matter-radiation equality. Here, we present the relation between the frequency $f = k/(2\pi)$ and T as [81]

$$\frac{f}{\text{nHz}} = 26.5 \left(\frac{T}{\text{GeV}} \right) \left(\frac{g_{*,\rho}(T)}{106.75} \right)^{\frac{1}{2}} \left(\frac{g_{*,s}(T)}{106.75} \right)^{-\frac{1}{3}}. \quad (14)$$

For the sake of illustration, we depict the energy-density fraction spectra of SIGWs in Fig. 1. The contribution of third-order tensor perturbations to the SIGW spectrum mainly occurs near the peak frequency, i.e., $k \sim k_*$, due to the resonance amplification, while its contribution in the lower frequency band is not particularly significant. If we fit the PTA data using the IR tail of the SIGW spectrum, analyses based on the SIGW spectrum with and without third-order tensor perturbations are expected to yield almost identical constraint results [37]. However, due to the significant enhancement of the SIGW spectrum near the peak frequency, the total energy-density fraction will be correspondingly increased. We therefore anticipate that cosmological data such as CMB and BAO will impose tight constraints on this effect [55, 57]. Based on the above reasons, by combining CMB, BAO, and PTA observational data, we expect to derive new constraints on the SIGW spectrum, thereby possibly suppressing both A_ζ and k_* .

C. Total energy-density fraction

The total physical energy-density fraction of SIGWs in the present-day universe is defined by an integral of the form

$$\omega_t \equiv \omega_t^{(2)} + \omega_t^{(3)} = \int_{f_{\min}}^{\infty} h^2 \Omega_{\text{GW},0}(2\pi f) d \ln f, \quad (15)$$

where the lower boundary is $f_{\min} \simeq 3 \times 10^{-17}$ for the CMB [53]. Here, the components $\omega_t^{(2)}$ and $\omega_t^{(3)}$, respectively, represent contributions from the second- and third-order tensor perturbations.

In addition, we further introduce their ratio of the form

$$R = \frac{\omega_t^{(3)}}{\omega_t^{(2)}}. \quad (16)$$

When they contribute equally to the SIGWs, namely $R = 1$, we find the critical value of $A_\zeta \simeq 0.06$, above which the third-order contribution is dominant, otherwise not. When discussing the formation of PBHs, A_ζ is usually required to be on the order of magnitude of $\mathcal{O}(10^{-2}-10^{-1})$ [16]. This indicates that, compared to second-order tensor perturbations, the contribution of third-order tensor perturbations is also non-negligible.

III. PERFORMANCE OF SIGW INTERPRETATION OF PTA DATA

In this section, we first analyze the CMB and BAO datasets to obtain the posteriors of ω_t . Then, we analyze the PTA data and incorporate the obtained posteriors of ω_t as a prior of ω_t into the likelihood related to PTA. Finally, we derive constraints on the parameters associated with SIGWs and then the primordial power-spectral amplitude and index using the dataset comprised of CMB, BAO, and PTA.

A. Cosmological analysis and results

Here, we derive the upper limits on ω_t via analyzing the CMB and BAO observational and mock datasets, respectively.

1. Cosmological model

The SIGWs are expected to leave detectable imprints on cosmological probes such as the CMB and BAO [54, 55]. Under the short-wavelength approximation, SIGWs can act as an additional energy component in the universe, altering the expansion rate of the early universe and thereby delaying the epoch of matter-radiation equality. This effect will change the size of the acoustic horizon during recombination. On the other hand, fluctuations in the energy density of SIGWs can affect the time derivative of scalar metric perturbations. This effect will influence the evolution of photon and matter perturbations, leaving detectable signatures in their power spectra. Furthermore, we adopt homogeneous initial conditions for the SIGW energy-density fluctuations [54, 55, 82]. Based on the above considerations, we can use the latest CMB and BAO datasets to constrain the independent parameter ω_t .

We study the so-called $w_0 w_a \text{CDM} + \omega_t$ model here. Apart from the independent parameter ω_t , this model also has eight additional independent parameters to be inferred. Specifically, ω_b and ω_c represent the present-day physical density fractions of baryons and cold dark matter, respectively. θ_{MC} is defined as the ratio of the sound horizon to the angular diameter distance at the epoch of decoupling. τ indicates the Thomson scattering optical depth resulting from reionization. A_s and n_s , respectively, signify the power-spectral amplitude and index of primordial curvature perturbations at the pivot scale $k_p = 0.05 \text{ Mpc}^{-1}$. w_0 and w_a are used to characterize the dynamical dark

energy with the equation of state of the form [83, 84]

$$w(a) = w_0 + w_a(1 - a), \quad (17)$$

where a is the scale factor of the universe. Here, we utilize the Cosmic Linear Anisotropy Solving System (CLASS) [85] code to generate cosmological models considered in this work.

2. Data analysis

To get observational constraints on ω_t from current cosmological data, the following combination of the CMB and BAO data is analyzed. For the CMB, we utilize the CMB-SPA data combination, as revealed in detail by Tab. III of Ref. [66]. It incorporates the cutting-edge measurements of the CMB temperature anisotropies, polarization, and lensing released by the *Planck* satellite, the South Pole Telescope (SPT-3G), and the Atacama Cosmology Telescope (ACT) [64–68]. Further, we use the recently released BAO data from the Dark Energy Spectroscopic Instrument (DESI) Data Release 2 (DR2) [56]. Here, we consider a uniform prior for ω_t , namely $\omega_t \in [0, 4 \times 10^{-6}]$. Other priors would not significantly change the leading results of this work. In addition, we adopt the `Cobaya` code [86] for parameter inference following the Markov-Chain Monte-Carlo (MCMC) method.

To get prospective constraints on ω_t from future observations, we consider next-generation experiments that are designed to achieve higher precision. Specifically, we utilize the Lite satellite for the study of B-mode polarization and Inflation from cosmic background Radiation Detection (LiteBIRD) [69] and the CMB Stage-IV (S4) [70] ground array for the CMB observations, while we use the China Space Station Telescope (CSST) [71, 72] for the BAO measurements. Following the approach of Refs. [57, 87, 88], we utilize the mock likelihood of LiteBIRD for the CMB observations at large angular scales ($2 \leq \ell \leq 50$), and that of S4 at small angular scales ($\ell > 50$). Further, we utilize the pessimistic precision of CSST for the BAO measurements, as revealed by Tab. 3 of Ref. [72], indicating conservative constraints on ω_t . Here, the fiducial model is given by the best-fit parameters inferred from the current cosmological observations, but the fiducial value of ω_t is assumed to be vanishing. In addition, we adopt the `MontePython` code [87, 88] for parameter inference following the MCMC method.

3. Results

In Fig. 2, we present the one-dimensional posterior distributions for ω_t , inferred from the observational data (blue curve) and the mock data (orange curve), respectively. In both cases, the 95% CL upper limits on ω_t are of order $\sim 10^{-7}$. Notably, the posterior derived from the mock data yields tighter constraints on ω_t than that obtained from the observational data. In the following analysis, we will incorporate these posterior results as priors on ω_t into the code used to analyze nanohertz gravitational-wave data from PTA observations, as demonstrated in the following subsection. This will allow a combined analysis of the latest CMB, BAO, and PTA datasets to infer parameters associated with SIGWs. Through this approach, we aim to clarify the physical

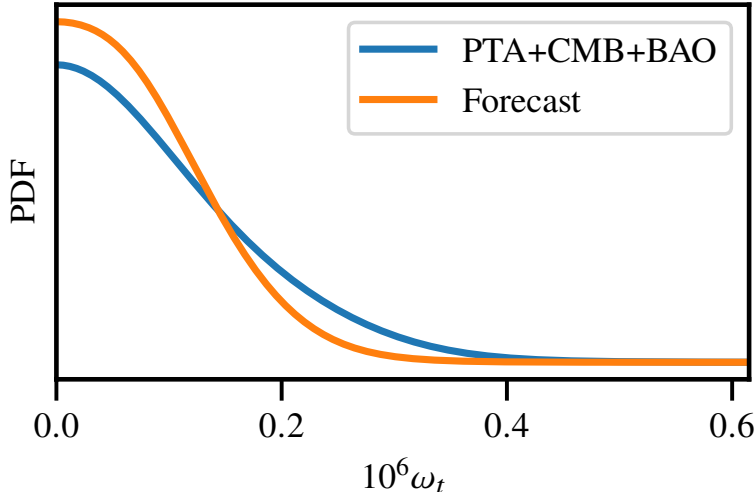


FIG. 2. One-dimensional posterior distributions of ω_t obtained via analyzing the CMB-SPA and DESI DR2 observational data (blue) and the LiteBIRD, S4, and CSST mock data (orange).

origin of the nanohertz gravitational-wave signal, that is, to determine whether it is cosmological or astrophysical in nature.

B. Methodology incorporating PTA data

We describe the procedure for incorporating PTA observations into our joint data analysis. For a given model of the GWB, whether cosmological, astrophysical, or a combination thereof, we analyze the NANOGrav 15yr dataset [1], which currently provides the highest statistical confidence among available PTA data releases. Following the standard methodology of PTA collaborations [7], we perform Bayesian parameter inference using the `Ceffy1` code [89]. The same analysis framework can be directly applied to other PTA datasets [2–4] as needed.

Regarding the theoretical interpretation of PTA data, we will consider two distinct models. The first model solely includes SIGWs, while the second model incorporates not only SIGWs but also a GWB component contributed by supermassive BHBs. For the former, its energy-density fraction spectrum has already been given in Eq. (13). For the latter, it should further include the energy-density fraction spectrum of the GWB generated by supermassive BHBs that are unresolved individually by PTA instruments. This spectrum is typically assumed to follow a power law of the form [6, 90]

$$\Omega_{\text{BHB}}(f) = \frac{2\pi^2 f_{\text{yr}}^2}{3H_0^2} A_{\text{BHB}}^2 \left(\frac{f}{f_{\text{yr}}} \right)^{5-\gamma_{\text{BHB}}}, \quad (18)$$

where A_{BHB} and γ_{BHB} , respectively, represent the spectral amplitude and index to be inferred here, f_{yr} denotes a pivot frequency corresponding to one year, and H_0 is the Hubble constant. Therefore, the total spectrum can be expressed as the sum of Eq. (13) and Eq. (18).

Here, we summarize the model parameters and their prior distributions used in this work. For models involving only SIGWs, there are two independent parameters, i.e., the amplitude A_ζ and

the characteristic frequency f_* , as defined in Eq. (4). For convenience, we use the corresponding wavenumber $k_* = 2\pi f_*$. We adopt uniform (log-flat) priors, namely $\log_{10} A_\zeta \in \mathcal{U}(-3, 1)$ and $\log_{10}(f_*/\text{Hz}) \in \mathcal{U}(-8, -5)$. For models involving both SIGWs and BHBs, we include the two astrophysical parameters A_{BHB} and γ_{BHB} from Eq. (18), in addition to the primordial parameters above (with identical priors). The priors for $\log_{10} A_{\text{BHB}}$ and γ_{BHB} are taken from Ref. [7] and are implemented as a bivariate normal distribution.

When studying SIGWs, which are of cosmological origin, the corresponding models are constrained not only by the PTA observations, but also by the CMB and BAO data. It is therefore necessary to perform a joint analysis of these complementary datasets. Specifically, in addition to the cosmological data analyzed in the previous subsection, we incorporate PTA observations to jointly constrain the model parameters. To this end, we introduce an informative prior on ω_t within the `Ceffyl` code [89], adopting the posterior distributions of ω_t derived in Fig. 2. This modification enables a consistent Bayesian inference using the combined dataset.

In order to perform model comparison, we use the Bayes factor, defined as [91, 92]

$$\mathcal{B}_{\alpha\beta} = \frac{p(d|\mathcal{M}_\alpha)}{p(d|\mathcal{M}_\beta)} = \frac{\int p(d|\theta_\alpha, \mathcal{M}_\alpha) \pi(\theta_\alpha|\mathcal{M}_\alpha) d\theta_\alpha}{\int p(d|\theta_\beta, \mathcal{M}_\beta) \pi(\theta_\beta|\mathcal{M}_\beta) d\theta_\beta}, \quad (19)$$

where d denotes the observed data, \mathcal{M}_α and \mathcal{M}_β represent two models under consideration, $p(d|\mathcal{M}_\alpha)$ is the Bayesian evidence for \mathcal{M}_α , $p(d|\theta_\alpha, \mathcal{M}_\alpha)$ is the likelihood function, and $\pi(\theta_\alpha|\mathcal{M}_\alpha)$ denotes the prior distribution for the model parameters θ_α in \mathcal{M}_α . To evaluate the performance of the SIGW interpretation of the PTA signal, we select \mathcal{M}_β as the baseline model containing only BHBs. In addition, we adopt the Jeffreys scale for interpreting the strength of evidence based on the Bayes factor, as outlined in Ref. [92]. Specifically, a value of $\mathcal{B}_{\alpha\beta} > 1$ supports \mathcal{M}_α over \mathcal{M}_β , with the evidence considered ‘not worth more than a bare mention’ for $1 < \mathcal{B}_{\alpha\beta} < 10^{1/2}$, substantial for $10^{1/2} < \mathcal{B}_{\alpha\beta} < 10$, strong for $10 < \mathcal{B}_{\alpha\beta} < 10^{3/2}$, very strong for $10^{3/2} < \mathcal{B}_{\alpha\beta} < 10^2$, and decisive for $\mathcal{B}_{\alpha\beta} > 10^2$. Conversely, $\mathcal{B}_{\alpha\beta} < 1$ indicates a preference for \mathcal{M}_β over \mathcal{M}_α , and the same descriptive scale applies to the reciprocal $\mathcal{B}_{\beta\alpha} = 1/\mathcal{B}_{\alpha\beta}$. When $\mathcal{B}_{\alpha\beta} = 1$, both models provide an equally good fit to the data.

C. Results from combined datasets

Here, we show the constraints on model parameters inferred from the aforementioned observational and mock datasets, respectively.

1. Observational constraints

Based on joint fits to the PTA, CMB, and BAO observations for the models considered in this work, we report the parameter constraints in Tab. I. This table lists the median values and 68% credible intervals (or the 95% credible lower limits where applicable) for the independent model parameters. The corresponding one- and two-dimensional posterior distributions are shown in Fig. 3. Here, the dark and light shaded regions, respectively, stand for 68% CL and 95% CL, while the dashed vertical lines represent 68% CL boundaries.

Model	Dataset	$\log_{10} A_\zeta$	$\log_{10} f_*$ [Hz]	$\log_{10} A_{\text{BHB}}$	γ_{BHB}	$\mathcal{B}_{\alpha\beta}$
SIGW	PTA	> -1.53	> -7.07	/	/	154.50
	+CMB+BAO	$-1.38^{+0.15}_{-0.18}$	$-6.86^{+0.22}_{-0.26}$	/	/	28.88
+BHB	PTA	> -1.56	> -7.08	$-15.75^{+0.42}_{-0.47}$	$4.66^{+0.34}_{-0.34}$	121.50
	+CMB+BAO	$-1.39^{+0.16}_{-0.19}$	$-6.85^{+0.23}_{-0.27}$	$-15.72^{+0.46}_{-0.48}$	$4.64^{+0.35}_{-0.35}$	23.77

TABLE I. Median values and 68% CL uncertainties (or the 95% credible lower limits where applicable) for the independent model parameters inferred from the joint data analysis. When estimating the Bayes factors, \mathcal{M}_α is identified with the model represented by each row of this table, and \mathcal{M}_β is selected as the baseline model containing only BHBs.

We find that when using only the PTA data to constrain either the SIGW model or the SIGW+BHB model, we obtain only lower limits for the cosmological parameters A_ζ and f_* , while their upper bounds reach the prior boundaries and thus cannot be effectively constrained. When we plot the SIGW spectrum corresponding to the central values of A_ζ and f_* in Fig. 1, we immediately notice that the peak of this spectrum does not lie within the gravitational-wave frequency band detectable by PTAs, but is higher by around one order of magnitude. In fact, when fitting the SIGW spectrum with PTA data, we are essentially fitting its IR tail. However, the spectral index of this IR tail is universal [93–95]. Therefore, it is difficult to constrain A_ζ , and consequently the range of f_* , using PTA data alone.

In comparison, the combination of PTA data with CMB and BAO observations yields well-constrained posterior distributions for both parameters, with bounds that are fully contained within the prior ranges. This enhanced constraining power stems from the ability of CMB and BAO data to limit the energy-density fraction of SIGWs. Joint analysis with PTA data thereby significantly reduces the allowable parameter interval for A_ζ , leading to substantially tighter constraints. Notably, the strong limitation placed on the upper bound of A_ζ further restricts the compatible range of f_* due to the positive correlation between the two parameters.

Based on the estimated results for the Bayes factors, we find that the data show a preference for the models containing the SIGW component over the model consisting solely of the astrophysical gravitational waves from BHBs. In particular, using PTA data alone yields decisive evidence in favor of the models involving SIGWs. However, when PTA data are combined with the CMB and BAO observations, the corresponding Bayes factors decrease significantly to a level of strong evidence. This phenomenon reflects the balance between model fit and the added data when assessing the overall evidence. Therefore, based on current data, it cannot be definitively concluded whether the PTA signal contains a SIGW component. A more conclusive assessment will require future observations with improved precision, e.g., the PTAs of the Square Kilometre Array (SKA) [96–99] and the FAST Core Array [100].

Moreover, when fitting to the same observational dataset, we find that different models do not significantly shift the posterior distributions of the model parameters, nor do they substantially change the qualitative level of support from the Bayesian evidence, although the Bayes factor decreases somewhat after including the astrophysical gravitational-wave contribution from BHBs. This indicates strong robustness in our analysis outcomes.

Finally, we reiterate the importance of including the third-order gravitational-wave contribution

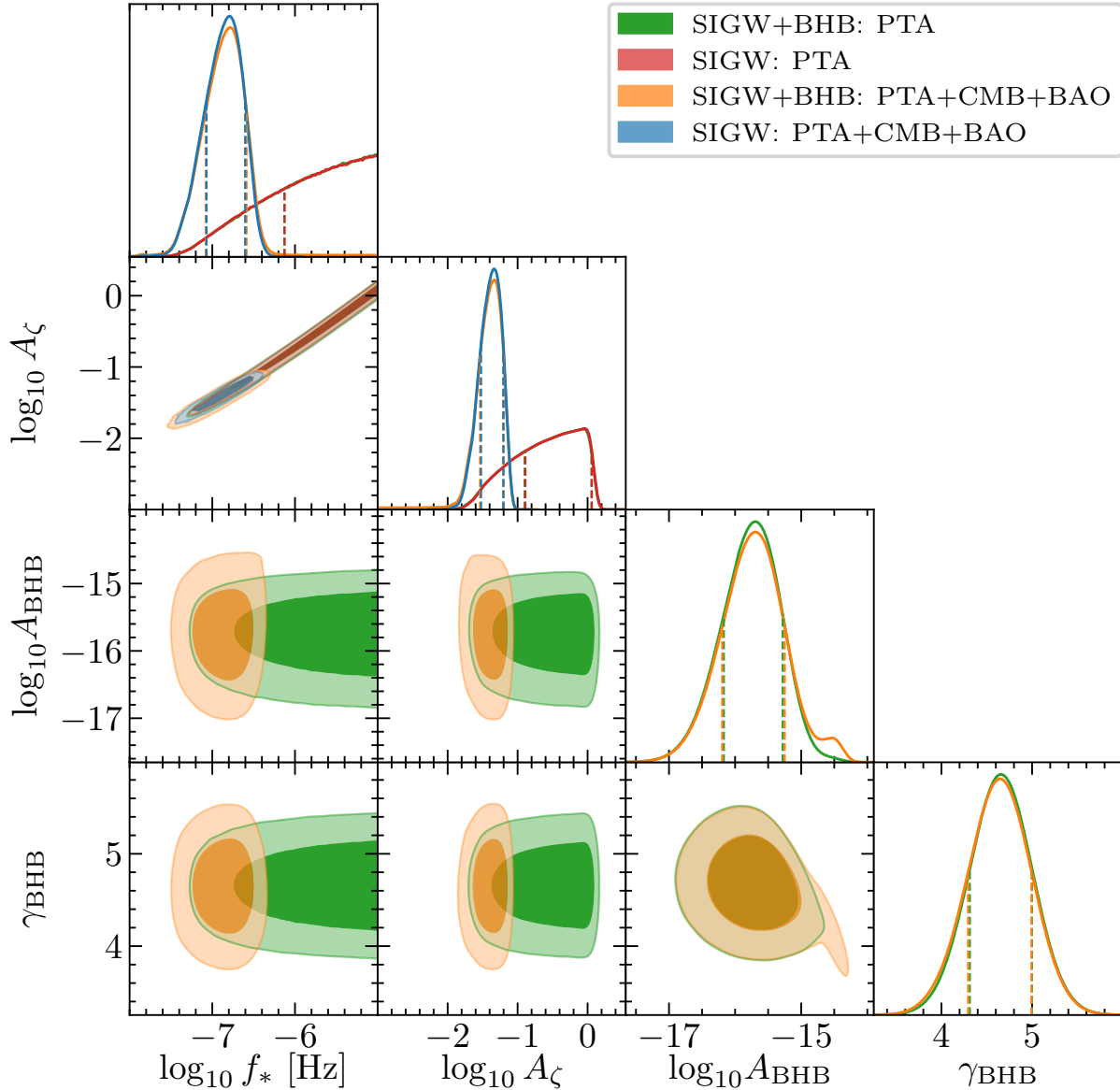


FIG. 3. One- and two-dimensional posterior distributions of the independent parameters inferred from the joint data analysis. Dark and light shaded regions, respectively, stand for 68% and 95% CL. Dashed vertical lines represent 68% CL boundaries.

in interpreting the PTA data. While it was found in the literature [7] that PTA data alone provide very strong evidence for the SIGW interpretation when only the second-order gravitational waves are considered, our present work, which incorporates both second- and third-order contributions, finds that the PTA data yield decisive evidence in favor of the SIGW scenario. This evidence, however, is reduced to the level of strong evidence once cosmological datasets are included in the analysis.

2. Prospective constraints

When fitting the future observations to the models considered in this work, we report the prospective parameter constraints in Tab. II. This table lists the median values and 68% credible intervals for the independent model parameters. The corresponding one- and two-dimensional posterior distributions are shown in Fig. 4. Here, the dark and light shaded regions, respectively, still stand for 68% CL and 95% CL, while the dashed vertical lines represent 68% CL boundaries.

Model	$\log_{10} A_\zeta$	$\log_{10} f_*$ [Hz]	$\log_{10} A_{\text{BHB}}$	γ_{BHB}
SIGW	$-1.40^{+0.14}_{-0.17}$	$-6.89^{+0.21}_{-0.25}$	/	/
+BHB	$-1.41^{+0.15}_{-0.18}$	$-6.88^{+0.22}_{-0.26}$	$-15.72^{+0.47}_{-0.48}$	$4.64^{+0.35}_{-0.36}$

TABLE II. The same as Tab. I, but we use the mock data of the next-generation CMB and BAO experiments.

Comparing Tab. II to Tab. I, we find that the next-generation CMB and BAO observations do not substantially reduce the allowed parameter space of the models considered here, as further revealed by Fig. 4. In fact, as shown in Fig. 2, these observations do not significantly alter the constraint on the energy-density fraction of the cosmological GWB, i.e., ω_t (changing it by less than $\sim 10\%$), which in turn is used to constrain the SIGW-related parameters. Therefore, we can expect that these data will not lead to a notable tightening of the constraints on those parameters either.

However, it should be emphasized that although our analysis employs the next-generation CMB and BAO observations, the resulting prospective constraints are not derived from future, more precise PTA data, but rather from the current NANOGrav 15yr dataset. In the upcoming future, observations from the SKA and the FAST Core Array are expected to deliver significantly-improved PTA measurements, which should help to effectively discriminate between different physical origins of the nanohertz GWB. Furthermore, we note that 21-cm line observations [101], which will provide precise measurements of the large-scale structures of the universe [102–106] and thus place tight constraints on cosmological models, are expected to effectively constrain ω_t as well. We expect that this can further strengthen the constraining power on SIGW-related models. Such an investigation, however, lies beyond the scope of the present work and will be explored in detail in future studies.

IV. IMPLICATIONS FOR PBH OVERPRODUCTION PROBLEM

When interpreting the PTA signal in the framework of SIGWs, the enhancement of the energy-density spectrum of SIGWs due to involvement of third-order components results in a suppression of A_ζ . This amplitude reduction provides a possible resolution to the PBH overproduction problem, given the exponential sensitivity of PBH abundance to curvature perturbations, i.e., $f_{\text{PBH}} \sim \exp(-1/(2A_\zeta))$ [107, 108]. Here, our analysis demonstrates that the parameter region favored by the combined dataset possibly yields cosmologically acceptable PBH abundances, leading to potential reconciliation of the PBH overproduction problem.

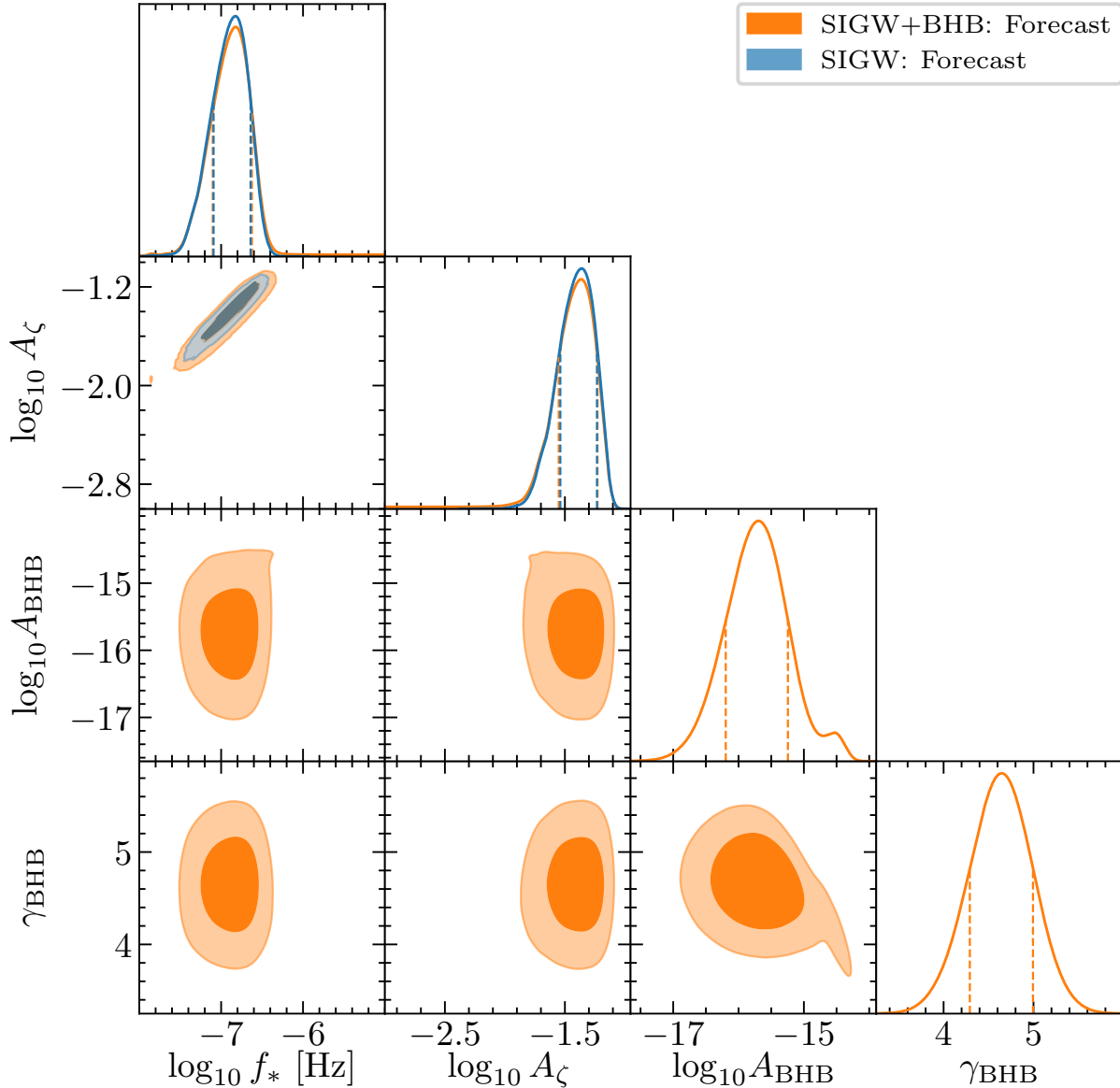


FIG. 4. The same as Fig. 3, but we use the mock data of the next-generation CMB and BAO experiments.

A. Formulas for PBH abundance

The PBH abundance is an integral of the PBH mass function $F_{\text{PBH}}(m)$ over the PBH mass m , namely,

$$f_{\text{PBH}} = \int F_{\text{PBH}}(m) d \ln m. \quad (20)$$

Following the theory of critical collapse [109, 110] and the Press-Schechter formalism [111], we get the PBH mass function, i.e., [81]

$$F_{\text{PBH}}(m) = \frac{\Omega_m}{\Omega_{dm}} \int \tilde{\beta}(m, m_H) g(T(m_H)) d \ln m_H, \quad (21)$$

where Ω_m and Ω_{dm} , respectively, stand for the present-day energy-density fraction of non-relativistic matter and dark matter, m_H is the mass within the Hubble horizon. For the sake of simplicity, we introduce

$$g(T) = \frac{g_{*,\rho}(T)}{g_{*,\rho}(T_{\text{eq}})} \frac{g_{*,s}(T_{\text{eq}})}{g_{*,s}(T)} \frac{T}{T_{\text{eq}}}, \quad (22)$$

$$\tilde{\beta}(m, m_H) = \frac{\kappa \mu^{\gamma+1}}{\sqrt{2\pi\gamma}\Delta(k)} \exp\left(-\frac{(\delta_c + \mu)^2}{2\Delta^2(k)}\right), \quad (23)$$

where $\mu = [m/(\kappa m_H)]^{1/\gamma}$ has constants $\kappa = 3.3$ [112] and $\gamma = 0.36$ [113–117], the critical overdensity for the gravitational collapse is $\delta_c = 0.45$ [115–117], and both $g_{*,\rho}$ and $g_{*,s}$ represent the effective numbers of relativistic degrees of freedom [80]. Here, we can get $T(m_H)$ via reversing the relation between m_H and T , namely [78],

$$\frac{m_H}{M_\odot} = 4.76 \times 10^{-2} \left(\frac{T}{\text{GeV}}\right)^{-2} \left(\frac{g_{*,\rho}(T)}{106.75}\right)^{-\frac{1}{2}}, \quad (24)$$

where M_\odot denotes the mass of the Sun. Moreover, the coarse-grained perturbations during radiation domination are given by [118, 119]

$$\Delta^2(k) = \frac{16}{81} \int \left(\frac{q}{k}\right)^4 w^2\left(\frac{q}{k}\right) \mathcal{T}^2\left(q, \frac{1}{k}\right) \mathcal{P}_\zeta(q) d\ln q, \quad (25)$$

where $w(y) = \exp(-y^2/2)$ is the Gaussian window function, and $\mathcal{T}(q, \tau) = 3(\sin x - x \cos x)/x^3$ with $x = q\tau/\sqrt{3}$ is the scalar transfer function.

Based on the formulas presented here, for each value of $k_* = 2\pi f_*$, we can derive the corresponding value of A_ζ for which $f_{\text{PBH}} = 1$. In Fig. 5, the black dashed curves represent this $f_{\text{PBH}} = 1$ contour. The parameter regions above the curves correspond to the overproduction of PBHs.

B. Towards solving PBH overproduction problem

In Fig. 5, we further compare the two-dimensional posterior distributions of A_ζ and f_* obtained in Subsection III C with the $f_{\text{PBH}} = 1$ contour. Here, we depict the left panel using the posteriors derived from the current observations, as shown in Fig. 3, while the right panel uses those from the future observations, as shown in Fig. 4.

As shown in the left panel of Fig. 5, when only PTA data are used, the parameter space favored by the data for the SIGW interpretation of the PTA signal, regardless of whether the BHBs background is included, leads to an overproduction of PBHs. This indicates an internal tension in the theoretical model under this interpretation. This result is consistent with earlier findings in the literature (e.g., Ref. [7]), which reported the same issue when considering only second-order gravitational waves. Our present work, which includes both second- and third-order contributions, confirms that the PBH overproduction problem is substantially alleviated but not completely resolved. The underlying reason is that the fit to the PTA data in the SIGW scenario relies primarily on the universal IR tail of the SIGW spectrum (illustrated previously in, e.g., Fig. 1). Because this tail has a universal spectral index, the PTA data cannot effectively constrain the upper bound of A_ζ . Due to the positive correlation between A_ζ and f_* , the upper bound of f_*

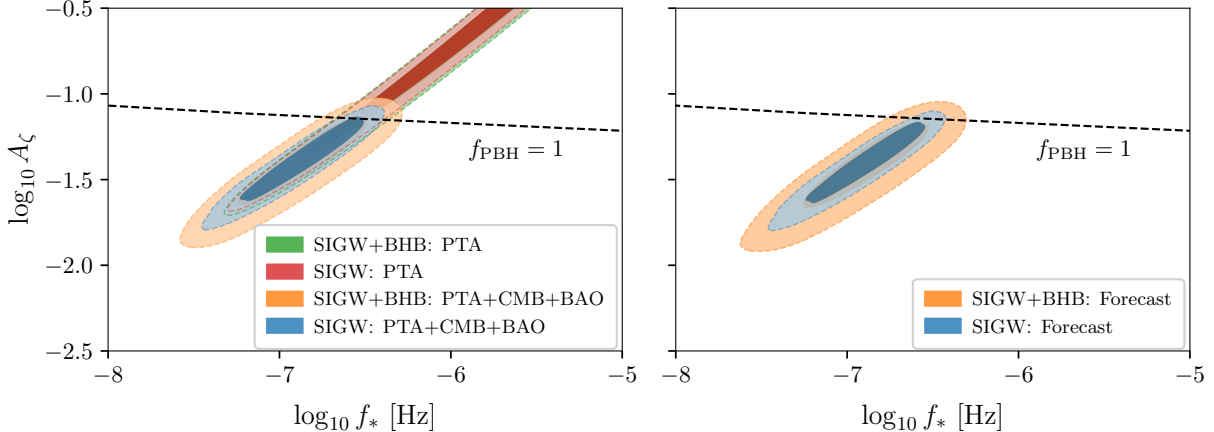


FIG. 5. Two-dimensional posterior distributions of A_ζ and f_* versus the $f_{\text{PBH}} = 1$ contour. We depict the left/right panel using the posteriors derived in Fig. 3/ Fig. 4. For comparison, we depict the $f_{\text{PBH}} = 1$ contour in black dashed curves.

also remains unconstrained. Consequently, the allowed parameter space permits excessively large primordial curvature perturbations, which upon re-entering the Hubble horizon would produce an overabundance of PBHs.

However, when CMB and BAO data are incorporated alongside the PTA measurements, the allowed parameter space is significantly reduced. Specifically, A_ζ becomes well-constrained, and consequently, so does f_* . In this case, the $f_{\text{PBH}} = 1$ contour only marginally touches the 68% CL region of the two-dimensional posterior distribution of the model parameters, which substantially alleviates (though does not completely resolve) the PBH overproduction problem. This improvement occurs because the CMB and BAO datasets tightly constrain the total energy-density fraction of the cosmological SIGWs background, thereby imposing a stringent upper limit on A_ζ and avoiding parameter regions that would produce an overabundance of PBHs. Finally, we reiterate that a consistent interpretation of the PTA signal within the SIGW framework must account for the third-order gravitational-wave contribution, as it becomes comparably important to the second-order contribution when $A_\zeta \sim \mathcal{O}(10^{-2} - 10^{-1})$.

As demonstrated in the right panel of Fig. 5, the next-generation CMB and BAO observations are expected to further lower the upper bound on A_ζ , thereby providing additional mitigation of the PBH overproduction issue, though the improvement is relatively modest, with the $f_{\text{PBH}} = 1$ contour separated from the 1σ credible region of the two-dimensional posterior by only about 1.3σ . It should be noted, however, that while future CMB and BAO data are used here, the PTA dataset remains NANOGrav 15yr rather than a future PTA measurement. Should the precision of PTA instruments improve in the future, the quantitative conclusions of this study may change accordingly. Nevertheless, if one aims to investigate the SIGW interpretation of the PTA signal and the associated PBH overproduction problem, relying solely on PTA data remains insufficient. Other cosmological probes, such as 21-cm line observations [101], will continue to be essential. As

noted earlier, exploring these possibilities falls beyond the scope of the present work and is left for future study.

V. CONCLUSIONS AND DISCUSSION

In this work, we performed a comprehensive Bayesian analysis to reassess the SIGW interpretation of the nanohertz GWB reported by PTAs, with particular attention to the associated PBH overproduction problem. By consistently incorporating both second- and third-order contributions to the SIGW spectrum, and employing a joint dataset comprising CMB, BAO, and PTA (i.e., NANOGrav 15yr) observations, we derived new constraints on the key parameters of the primordial curvature power spectrum—the amplitude A_ζ and the characteristic frequency f_* . Our analysis demonstrated that the inclusion of third-order gravitational waves, which become significant for $A_\zeta \sim \mathcal{O}(10^{-2} - 10^{-1})$, substantially enhanced the spectral amplitude of SIGWs. This enhancement allowed the PTA signal to be fitted with a lower required curvature perturbation amplitude, thereby providing a crucial mechanism to alleviate the tension with PBH overproduction limits. The joint analysis revealed that while PTA data alone favored the SIGW interpretation decisively, the combination with CMB and BAO data tightened the constraints on the model parameters significantly, reducing the evidence to the level of "strong" and offering a parameter space where the implied PBH abundance could be cosmologically acceptable.

The integration of cosmological data proved essential for breaking degeneracies inherent in the PTA-only analysis. We found that CMB and BAO observations imposed a stringent upper limit on the total energy-density fraction of cosmological gravitational waves, ω_t . This external constraint, when combined with PTA data, effectively restricted the upper bounds of both A_ζ and f_* , which were positively correlated. Consequently, the parameter region preferred by the combined data shifted away from the regime that would lead to an overabundance of PBHs, as defined by the $f_{\text{PBH}} = 1$ contour. Although the PBH overproduction problem was not completely resolved, with the $f_{\text{PBH}} = 1$ contour remaining close to the 1σ credible region of the posterior, the tension was substantially mitigated. This outcome underscored the importance of multi-messenger cosmology, where late-universe anchors from CMB and BAO were indispensable for pinning down early-universe parameters inferred from gravitational-wave observations.

In principle, the analysis presented in this study should further consider the contributions of gravitational waves beyond the third order. To our knowledge, such analyses are absent in the literature due to the extreme complexity arising from the nonlinear nature of general relativity. However, it can be anticipated that the contributions of higher-order gravitational waves to the cosmological gravitational-wave background always correspond to a positive definite energy density. Therefore, the constraints on the primordial curvature power spectrum derived in this study would become more stringent, leading to tighter constraints on PBHs. This could further alleviate the overproduction problem of PBHs.

A caveat in this study is that the quantitative severity of PBH overproduction is not fully model independent. In PTA-motivated SIGW interpretations, the inferred PBH abundance can shift appreciably when assumptions about primordial non-Gaussianity or the equation of state of the early Universe are changed [17–19, 33, 34, 38, 120–128]. Moreover, this work does not account

for evolutionary effects on the PBH mass function induced by mergers [7, 129] or by accretion. In particular, for PBHs with masses above a few solar masses, accretion can substantially weaken observational constraints [7, 130, 131], whereas for sub-solar-mass PBHs the impact of accretion is expected to be small [7, 131]. Therefore, the alleviation found in this work should be interpreted within the adopted PBH-formation framework, while a sharper conclusion will require further progress on the PBH theory side.

Looking ahead, our study highlights several promising directions for future research. Prospective constraints from next-generation CMB and BAO experiments are expected to provide only a modest further reduction in the allowed parameter space. A more decisive resolution of the PTA signal's origin and the PBH overproduction issue will likely require significantly improved PTA measurements, such as those anticipated from the SKA and the FAST Core Array. Furthermore, complementary probes like 21-cm line surveys, which will deliver precise measurements of large-scale structures, hold great potential for independently constraining ω_t and thereby strengthening the limits on SIGW models. In addition, anisotropies of cosmological gravitational-wave backgrounds and their cross-correlations with the CMB and large-scale structures can provide complementary diagnostics of source origin and primordial non-Gaussianity. Our work, therefore, not only advances the current understanding of the SIGW interpretation and its theoretical consistency, but also provides a clear roadmap for future observational campaigns to definitively test the cosmological origin of the nanohertz GWB and its connection to PBHs.

ACKNOWLEDGMENTS

Z.C.Z. is supported by the National Key Research and Development Program of China Grant No. 2021YFC2203001. S.W. is supported by the National Natural Science Foundation of China (Grant No. 12533001). Q.H.Z. is supported by the National Natural Science Foundation of China (Grant Nos. 12305073, 12547101). X.Z. is supported by the National Natural Science Foundation of China (Grants Nos. 12473001, 12575049, 12533001), the National SKA Program of China (Grants Nos. 2022SKA0110200, 2022SKA0110203), the China Manned Space Program (Grant No. CMS-CSST-2025-A02). This study is supported by Advanced Computation Center of Hangzhou Normal University.

-
- [1] NANOGrav collaboration, *The NANOGrav 15-year Data Set: Evidence for a Gravitational-Wave Background*, *Astrophys. J. Lett.* **951** (2023) [2306.16213].
 - [2] EPTA, INPTA: collaboration, *The second data release from the European Pulsar Timing Array - III. Search for gravitational wave signals*, *Astron. Astrophys.* **678** (2023) A50 [2306.16214].
 - [3] D.J. Reardon et al., *Search for an isotropic gravitational-wave background with the Parkes Pulsar Timing Array*, *Astrophys. J. Lett.* **951** (2023) [2306.16215].
 - [4] H. Xu et al., *Searching for the Nano-Hertz Stochastic Gravitational Wave Background with the Chinese Pulsar Timing Array Data Release I*, *Res. Astron. Astrophys.* **23** (2023) 075024 [2306.16216].

- [5] EPTA, INPTA collaboration, *The second data release from the European Pulsar Timing Array - IV. Implications for massive black holes, dark matter, and the early Universe*, *Astron. Astrophys.* **685** (2024) A94 [2306.16227].
- [6] NANOGrav collaboration, *The NANOGrav 15 yr Data Set: Constraints on Supermassive Black Hole Binaries from the Gravitational-wave Background*, *Astrophys. J. Lett.* **952** (2023) L37 [2306.16220].
- [7] NANOGrav collaboration, *The NANOGrav 15 yr Data Set: Search for Signals from New Physics*, *Astrophys. J. Lett.* **951** (2023) L11 [2306.16219].
- [8] Y.-C. Bi, Y.-M. Wu, Z.-C. Chen and Q.-G. Huang, *Implications for the supermassive black hole binaries from the NANOGrav 15-year data set*, *Sci. China Phys. Mech. Astron.* **66** (2023) 120402 [2307.00722].
- [9] L. Bian et al., *Gravitational wave cosmology*, *Sci. China Phys. Mech. Astron.* **69** (2026) 210401 [2505.19747].
- [10] K.N. Ananda, C. Clarkson and D. Wands, *The Cosmological gravitational wave background from primordial density perturbations*, *Phys. Rev. D* **75** (2007) 123518 [gr-qc/0612013].
- [11] D. Baumann, P.J. Steinhardt, K. Takahashi and K. Ichiki, *Gravitational Wave Spectrum Induced by Primordial Scalar Perturbations*, *Phys. Rev. D* **76** (2007) 084019 [hep-th/0703290].
- [12] S. Mollerach, D. Harari and S. Matarrese, *CMB polarization from secondary vector and tensor modes*, *Phys. Rev. D* **69** (2004) 063002 [astro-ph/0310711].
- [13] H. Assadullahi and D. Wands, *Constraints on primordial density perturbations from induced gravitational waves*, *Phys. Rev. D* **81** (2010) 023527 [0907.4073].
- [14] J.R. Espinosa, D. Racco and A. Riotto, *A Cosmological Signature of the SM Higgs Instability: Gravitational Waves*, *JCAP* **09** (2018) 012 [1804.07732].
- [15] K. Kohri and T. Terada, *Semianalytic calculation of gravitational wave spectrum nonlinearly induced from primordial curvature perturbations*, *Phys. Rev. D* **97** (2018) 123532 [1804.08577].
- [16] B. Carr, K. Kohri, Y. Sendouda and J. Yokoyama, *Constraints on primordial black holes*, *Rept. Prog. Phys.* **84** (2021) 116902 [2002.12778].
- [17] G. Franciolini, A. Iovino, Junior., V. Vaskonen and H. Veermae, *Recent Gravitational Wave Observation by Pulsar Timing Arrays and Primordial Black Holes: The Importance of Non-Gaussianities*, *Phys. Rev. Lett.* **131** (2023) 201401 [2306.17149].
- [18] S. Wang, Z.-C. Zhao, J.-P. Li and Q.-H. Zhu, *Implications of pulsar timing array data for scalar-induced gravitational waves and primordial black holes: Primordial non-Gaussianity fNL considered*, *Phys. Rev. Res.* **6** (2024) L012060 [2307.00572].
- [19] L. Liu, Z.-C. Chen and Q.-G. Huang, *Implications for the non-Gaussianity of curvature perturbation from pulsar timing arrays*, *Phys. Rev. D* **109** (2024) L061301 [2307.01102].
- [20] Y.-F. Cai, X.-C. He, X.-H. Ma, S.-F. Yan and G.-W. Yuan, *Limits on scalar-induced gravitational waves from the stochastic background by pulsar timing array observations*, *Sci. Bull.* **68** (2023) 2929 [2306.17822].
- [21] K. Inomata, K. Kohri and T. Terada, *Detected stochastic gravitational waves and subsolar-mass primordial black holes*, *Phys. Rev. D* **109** (2024) 063506 [2306.17834].
- [22] K. Inomata, M. Kawasaki, K. Mukaida and T.T. Yanagida, *Axion curvaton model for the gravitational waves observed by pulsar timing arrays*, *Phys. Rev. D* **109** (2024) 043508 [2309.11398].
- [23] K.T. Abe and Y. Tada, *Translating nano-Hertz gravitational wave background into primordial perturbations taking account of the cosmological QCD phase transition*, *Phys. Rev. D* **108** (2023) L101304 [2307.01653].
- [24] Z. Yi, Q. Gao, Y. Gong, Y. Wang and F. Zhang, *Scalar induced gravitational waves in light of Pulsar Timing Array data*, *Sci. China Phys. Mech. Astron.* **66** (2023) 120404 [2307.02467].

- [25] J.-Z. Zhou, Y.-T. Kuang, Z. Chang, X. Zhang and Q.-H. Zhu, *Primordial black holes and scalar induced density perturbations: the effects of probability density functions**, *Chin. Phys. C* **49** (2025) 025105 [2307.02067].
- [26] H. Firouzjahi and A. Talebian, *Induced gravitational waves from ultra slow-roll inflation and pulsar timing arrays observations*, *JCAP* **10** (2023) 032 [2307.03164].
- [27] Z.-Q. You, Z. Yi and Y. Wu, *Constraints on primordial curvature power spectrum with pulsar timing arrays*, *JCAP* **11** (2023) 065 [2307.04419].
- [28] P. Bari, N. Bartolo, G. Domènech and S. Matarrese, *Gravitational waves induced by scalar-tensor mixing*, *Phys. Rev. D* **109** (2024) 023509 [2307.05404].
- [29] D.G. Figueroa, M. Pieroni, A. Ricciardone and P. Simakachorn, *Cosmological Background Interpretation of Pulsar Timing Array Data*, *Phys. Rev. Lett.* **132** (2024) 171002 [2307.02399].
- [30] K. Harigaya, K. Inomata and T. Terada, *Induced gravitational waves with kination era for recent pulsar timing array signals*, *Phys. Rev. D* **108** (2023) 123538 [2309.00228].
- [31] S. Balaji, G. Domènech and G. Franciolini, *Scalar-induced gravitational wave interpretation of PTA data: the role of scalar fluctuation propagation speed*, *JCAP* **10** (2023) 041 [2307.08552].
- [32] Z.-C. Chen, J. Li, L. Liu and Z. Yi, *Probing the speed of scalar-induced gravitational waves with pulsar timing arrays*, *Phys. Rev. D* **109** (2024) L101302 [2401.09818].
- [33] H. Firouzjahi and A. Riotto, *Sign of non-Gaussianity and the primordial black holes abundance*, *Phys. Rev. D* **108** (2023) 123504 [2309.10536].
- [34] S. Choudhury, K. Dey, A. Karde, S. Panda and M. Sami, *Primordial non-Gaussianity as a saviour for PBH overproduction in SIGWs generated by pulsar timing arrays for Galileon inflation*, *Phys. Lett. B* **856** (2024) 138925 [2310.11034].
- [35] S. Choudhury, K. Dey and A. Karde, *Untangling PBH Overproduction in w -SIGWs Generated by Pulsar Timing Arrays for MST-EFT of Single Field Inflation*, *Fortsch. Phys.* **74** (2026) e70067 [2311.15065].
- [36] G. Domènech and A. Ganz, *Enhanced induced gravitational waves in Horndeski gravity*, *JCAP* **01** (2025) 020 [2406.19950].
- [37] S. Wang, Z.-C. Zhao and Q.-H. Zhu, *Constraints on scalar-induced gravitational waves up to third order from a joint analysis of BBN, CMB, and PTA data*, *Phys. Rev. Res.* **6** (2024) 013207 [2307.03095].
- [38] Q.-H. Zhu, Z.-C. Zhao, S. Wang and X. Zhang, *Unraveling the early universe's equation of state and primordial black hole production with PTA, BBN, and CMB observations**, *Chin. Phys. C* **48** (2024) 125105 [2307.13574].
- [39] J.-Z. Zhou, Y.-T. Kuang, Z. Chang and H. Lü, *Constraints on Primordial Black Holes from N_{eff} : Scalar-induced Gravitational Waves as an Extra Radiation Component*, *Astrophys. J.* **979** (2025) 178 [2410.10111].
- [40] J.-Z. Zhou, Z.-C. Li and D. Wu, *Cosmological constraints on small-scale primordial non-Gaussianity*, *Phys. Rev. D* **112** (2025) 063511 [2505.22614].
- [41] D. Wu, J.-Z. Zhou, Y.-T. Kuang, Z.-C. Li, Z. Chang and Q.-G. Huang, *Can tensor-scalar induced GWs dominate PTA observations?*, *JCAP* **03** (2025) 045 [2501.00228].
- [42] S. Choudhury, K. Dey, S. Ganguly, A. Karde, S.K. Singh and P. Tiwari, *Negative non-Gaussianity as a salvager for PBHs with PTAs in bounce*, *Eur. Phys. J. C* **85** (2025) 472 [2409.18983].
- [43] J. Jiang, J. Lin and X. Gao, *Scalar-induced gravitational waves in spatially covariant gravity*, 2508.20000.
- [44] J.-X. Feng, F. Zhang and X. Gao, *Scalar induced gravitational waves in chiral scalar-tensor theory of gravity*, *Eur. Phys. J. C* **84** (2024) 736 [2404.05289].
- [45] R. Roshan and G. White, *Using gravitational waves to see the first second of the Universe*, *Rev. Mod. Phys.* **97** (2025) 015001 [2401.04388].

- [46] G. Domènech, S. Pi and A. Wang, *A Unified Origin of Primordial Black Hole Dark Matter and Nanohertz Gravitational Waves*, 2602.24061.
- [47] C. Yuan, Z.-C. Chen and Q.-G. Huang, *Probing primordial–black-hole dark matter with scalar induced gravitational waves*, *Phys. Rev. D* **100** (2019) 8 [1906.11549].
- [48] J.-Z. Zhou, X. Zhang, Q.-H. Zhu and Z. Chang, *The third order scalar induced gravitational waves*, *JCAP* **05** (2022) 013 [2106.01641].
- [49] Z. Chang, Y.-T. Kuang, X. Zhang and J.-Z. Zhou, *Primordial black holes and third order scalar induced gravitational waves**, *Chin. Phys. C* **47** (2023) 055104 [2209.12404].
- [50] Z. Chang, Y.-T. Kuang, D. Wu and J.-Z. Zhou, *Probing scalar induced gravitational waves with PTA and LISA: the importance of third order correction*, *JCAP* **2024** (2024) 044 [2312.14409].
- [51] J.-Z. Zhou, Y.-T. Kuang, D. Wu, H. Lü and Z. Chang, *Induced gravitational waves for arbitrary higher orders: Vertex rules and loop diagrams in cosmological perturbation theory*, *Phys. Rev. D* **111** (2025) 083512 [2408.14052].
- [52] C.J. Moore and A. Vecchio, *Ultra-low-frequency gravitational waves from cosmological and astrophysical processes*, *Nature Astron.* **5** (2021) 1268 [2104.15130].
- [53] M. Maggiore, *Gravitational Waves. Vol. 2: Astrophysics and Cosmology*, Oxford University Press (3, 2018).
- [54] T.L. Smith, E. Pierpaoli and M. Kamionkowski, *A new cosmic microwave background constraint to primordial gravitational waves*, *Phys. Rev. Lett.* **97** (2006) 021301 [astro-ph/0603144].
- [55] T.J. Clarke, E.J. Copeland and A. Moss, *Constraints on primordial gravitational waves from the Cosmic Microwave Background*, *JCAP* **10** (2020) 002 [2004.11396].
- [56] DESI collaboration, *DESI DR2 results. II. Measurements of baryon acoustic oscillations and cosmological constraints*, *Phys. Rev. D* **112** (2025) 083515 [2503.14738].
- [57] S. Wang and Z.-C. Zhao, *New constraints on cosmological gravitational waves from CMB and BAO in light of dynamical dark energy**, *Chin. Phys.* **50** (2026) 025105 [2507.06930].
- [58] G. Cabass, L. Pagano, L. Salvati, M. Gerbino, E. Giusarma and A. Melchiorri, *Updated Constraints and Forecasts on Primordial Tensor Modes*, *Phys. Rev. D* **93** (2016) 063508 [1511.05146].
- [59] X.-J. Liu, W. Zhao, Y. Zhang and Z.-H. Zhu, *Detecting Relic Gravitational Waves by Pulsar Timing Arrays: Effects of Cosmic Phase Transitions and Relativistic Free-Streaming Gases*, *Phys. Rev. D* **93** (2016) 024031 [1509.03524].
- [60] S. Vagnozzi, *Inflationary interpretation of the stochastic gravitational wave background signal detected by pulsar timing array experiments*, *JHEAp* **39** (2023) 81 [2306.16912].
- [61] T. Bringmann, P.F. Depta, T. Konstandin, K. Schmidt-Hoberg and C. Tasillo, *Does NANOGrav observe a dark sector phase transition?*, *JCAP* **11** (2023) 053 [2306.09411].
- [62] M. Tagliacucchi, M. Braglia, F. Finelli and M. Pieroni, *Quest for CMB spectral distortions to probe the scalar-induced gravitational wave background interpretation of pulsar timing array data*, *Phys. Rev. D* **111** (2025) L021305 [2310.08527].
- [63] D. Wu, Z.-C. Li, P.-Y. Wu, F.-Y. Chen and J.-Z. Zhou, *Probing small-scale primordial power spectra with tensor-scalar induced gravitational waves*, 2507.07836.
- [64] J. Carron, M. Mirmelstein and A. Lewis, *CMB lensing from Planck PR4 maps*, *JCAP* **09** (2022) 039 [2206.07773].
- [65] SPT-3G collaboration, *Cosmology from CMB lensing and delensed EE power spectra using 2019–2020 SPT-3G polarization data*, *Phys. Rev. D* **111** (2025) 083534 [2411.06000].
- [66] SPT-3G collaboration, *SPT-3G D1: CMB temperature and polarization power spectra and cosmology from 2019 and 2020 observations of the SPT-3G Main field*, 2506.20707.
- [67] ACT, SPT-3G collaboration, *Unified and Consistent Structure Growth Measurements from Joint ACT, SPT, and Planck CMB Lensing*, *Phys. Rev. Lett.* **136** (2026) 021001 [2504.20038].

- [68] ATACAMA COSMOLOGY TELESCOPE collaboration, *The Atacama Cosmology Telescope: DR6 power spectra, likelihoods and Λ CDM parameters*, *JCAP* **11** (2025) 062 [2503.14452].
- [69] LITEBIRD collaboration, *Probing Cosmic Inflation with the LiteBIRD Cosmic Microwave Background Polarization Survey*, *PTEP* **2023** (2023) 042F01 [2202.02773].
- [70] CMB-S4 collaboration, *CMB-S4 Science Book, First Edition*, 1610.02743.
- [71] Y. Gong, X. Liu, Y. Cao, X. Chen, Z. Fan, R. Li et al., *Cosmology from the Chinese Space Station Optical Survey (CSS-OS)*, *Astrophys. J.* **883** (2019) 203 [1901.04634].
- [72] H. Miao, Y. Gong, X. Chen, Z. Huang, X.-D. Li and H. Zhan, *Forecasting the BAO measurements of the CSST galaxy and AGN spectroscopic surveys*, *Mon. Not. Roy. Astron. Soc.* **531** (2024) 3991 [2311.16903].
- [73] C.-P. Ma and E. Bertschinger, *Cosmological perturbation theory in the synchronous and conformal Newtonian gauges*, *Astrophys. J.* **455** (1995) 7 [astro-ph/9506072].
- [74] S. Dodelson, *Modern Cosmology*, Academic Press, Amsterdam (2003).
- [75] Y.-H. Yu and S. Wang, *Silk damping in scalar-induced gravitational waves: a novel probe for new physics*, *Sci. China Phys. Mech. Astron.* **68** (2025) 210412 [2405.02960].
- [76] Y.-H. Yu, Z. Chang and S. Wang, *Comprehensive analysis of dissipative effects in the induced gravitational waves*, *JCAP* **02** (2026) 011 [2510.18663].
- [77] G. Domènech and J. Chluba, *Regularizing the induced GW spectrum with dissipative effects*, *JCAP* **07** (2025) 034 [2503.13670].
- [78] S. Wang, T. Terada and K. Kohri, *Prospective constraints on the primordial black hole abundance from the stochastic gravitational-wave backgrounds produced by coalescing events and curvature perturbations*, *Phys. Rev. D* **99** (2019) 103531 [1903.05924].
- [79] PLANCK collaboration, *Planck 2018 results. VI. Cosmological parameters*, *Astron. Astrophys.* **641** (2020) A6 [1807.06209].
- [80] K. Saikawa and S. Shirai, *Primordial gravitational waves, precisely: The role of thermodynamics in the Standard Model*, *JCAP* **05** (2018) 035 [1803.01038].
- [81] Z.-C. Zhao and S. Wang, *Bayesian Implications for the Primordial Black Holes from NANOGrav's Pulsar-Timing Data Using the Scalar-Induced Gravitational Waves*, *Universe* **9** (2023) 157 [2211.09450].
- [82] M. Bucher, K. Moodley and N. Turok, *The General primordial cosmic perturbation*, *Phys. Rev. D* **62** (2000) 083508 [astro-ph/9904231].
- [83] M. Chevallier and D. Polarski, *Accelerating universes with scaling dark matter*, *Int. J. Mod. Phys. D* **10** (2001) 213 [gr-qc/0009008].
- [84] E.V. Linder, *Exploring the expansion history of the universe*, *Phys. Rev. Lett.* **90** (2003) 091301 [astro-ph/0208512].
- [85] D. Blas, J. Lesgourgues and T. Tram, *The Cosmic Linear Anisotropy Solving System (CLASS) II: Approximation schemes*, *JCAP* **07** (2011) 034 [1104.2933].
- [86] J. Torrado and A. Lewis, *Cobaya: Code for Bayesian Analysis of hierarchical physical models*, *JCAP* **05** (2021) 057 [2005.05290].
- [87] T. Brinckmann and J. Lesgourgues, *MontePython 3: boosted MCMC sampler and other features*, *Phys. Dark Univ.* **24** (2019) 100260 [1804.07261].
- [88] B. Audren, J. Lesgourgues, K. Benabed and S. Prunet, *Conservative Constraints on Early Cosmology: an illustration of the Monte Python cosmological parameter inference code*, *JCAP* **1302** (2013) 001 [1210.7183].
- [89] W.G. Lamb, S.R. Taylor and R. van Haasteren, *Rapid refitting techniques for Bayesian spectral characterization of the gravitational wave background using pulsar timing arrays*, *Phys. Rev. D* **108** (2023) 103019 [2303.15442].

- [90] EPTA, INPTA collaboration, *The second data release from the European Pulsar Timing Array - IV. Implications for massive black holes, dark matter, and the early Universe*, *Astron. Astrophys.* **685** (2024) A94 [2306.16227].
- [91] R.E. Kass and A.E. Raftery, *Bayes factors*, *Journal of the american statistical association* **90** (1995) 773.
- [92] H. Jeffreys, *The theory of probability*, OuP Oxford (1998).
- [93] R.-G. Cai, S. Pi and M. Sasaki, *Universal infrared scaling of gravitational wave background spectra*, *Phys. Rev. D* **102** (2020) 083528 [1909.13728].
- [94] C. Yuan, Z.-C. Chen and Q.-G. Huang, *Log-dependent slope of scalar induced gravitational waves in the infrared regions*, *Phys. Rev. D* **101** (2020) 4 [1910.09099].
- [95] J.-P. Li, S. Wang, Z.-C. Zhao and K. Kohri, *Isotropy, anisotropies and non-Gaussianity in the scalar-induced gravitational-wave background: diagrammatic approach for primordial non-Gaussianity up to arbitrary order*, 2505.16820.
- [96] SKAO PULSAR SCIENCE WORKING GROUP collaboration, *The SKAO Pulsar Timing Array*, 2512.16163.
- [97] L.-F. Wang, Y. Shao, S.-R. Xiao, J.-F. Zhang and X. Zhang, *Ultra-low-frequency gravitational waves from individual supermassive black hole binaries as standard sirens*, *JCAP* **05** (2025) 095 [2201.00607].
- [98] S.-R. Xiao, Y. Shao, L.-F. Wang, J.-Y. Song, L. Feng, J.-F. Zhang et al., *Nanohertz gravitational waves from a quasar-based supermassive black hole binary population model as dark sirens*, *JCAP* **04** (2025) 060 [2408.00609].
- [99] S.-R. Xiao, J.-Y. Song, Y. Shao, L.-F. Wang, J.-F. Zhang and X. Zhang, *Two-Dimensional Pulsar Distance Inference from Nanohertz Gravitational Waves*, 2512.10729.
- [100] P. Jiang, R. Chen, H. Gan, J. Sun, B. Zhu, H. Li et al., *The fast core array*, *Astronomical Techniques and Instruments* **1** (2024) 84.
- [101] J.R. Pritchard and A. Loeb, *21-cm cosmology*, *Rept. Prog. Phys.* **75** (2012) 086901 [1109.6012].
- [102] M. Zhang, B. Wang, P.-J. Wu, J.-Z. Qi, Y. Xu, J.-F. Zhang et al., *Prospects for Constraining Interacting Dark Energy Models with 21 cm Intensity Mapping Experiments*, *Astrophys. J.* **918** (2021) 56 [2102.03979].
- [103] P.-J. Wu and X. Zhang, *Prospects for measuring dark energy with 21 cm intensity mapping experiments*, *JCAP* **01** (2022) 060 [2108.03552].
- [104] P.-J. Wu, Y. Shao, S.-J. Jin and X. Zhang, *A path to precision cosmology: synergy between four promising late-universe cosmological probes*, *JCAP* **06** (2023) 052 [2202.09726].
- [105] P.-J. Wu, Y. Li, J.-F. Zhang and X. Zhang, *Prospects for measuring dark energy with 21 cm intensity mapping experiments: A joint survey strategy*, *Sci. China Phys. Mech. Astron.* **66** (2023) 270413 [2212.07681].
- [106] J.-D. Pan, P.-J. Wu, G.-H. Du, Y. Li and X. Zhang, *Prospects for cosmological research with the FAST array: 21-cm intensity mapping survey observation strategies*, *JCAP* **01** (2025) 080 [2408.00268].
- [107] A.M. Green and B.J. Kavanagh, *Primordial Black Holes as a dark matter candidate*, *J. Phys. G* **48** (2021) 043001 [2007.10722].
- [108] C.-M. Yoo, T. Harada, J. Garriga and K. Kohri, *Primordial black hole abundance from random Gaussian curvature perturbations and a local density threshold*, *PTEP* **2018** (2018) 123E01 [1805.03946].
- [109] J. Yokoyama, *Cosmological constraints on primordial black holes produced in the near critical gravitational collapse*, *Phys. Rev.* **D58** (1998) 107502 [gr-qc/9804041].
- [110] B. Carr, F. Kuhnel and M. Sandstad, *Primordial Black Holes as Dark Matter*, *Phys. Rev.* **D94** (2016) 083504 [1607.06077].

- [111] W.H. Press and P. Schechter, *Formation of galaxies and clusters of galaxies by selfsimilar gravitational condensation*, *Astrophys. J.* **187** (1974) 425.
- [112] J.C. Niemeyer and K. Jedamzik, *Near-critical gravitational collapse and the initial mass function of primordial black holes*, *Phys. Rev. Lett.* **80** (1998) 5481 [astro-ph/9709072].
- [113] T. Koike, T. Hara and S. Adachi, *Critical behavior in gravitational collapse of radiation fluid: A Renormalization group (linear perturbation) analysis*, *Phys. Rev. Lett.* **74** (1995) 5170 [gr-qc/9503007].
- [114] J.C. Niemeyer and K. Jedamzik, *Dynamics of primordial black hole formation*, *Phys. Rev. D* **59** (1999) 124013 [astro-ph/9901292].
- [115] I. Musco, J.C. Miller and L. Rezzolla, *Computations of primordial black hole formation*, *Class. Quant. Grav.* **22** (2005) 1405 [gr-qc/0412063].
- [116] I. Musco, J.C. Miller and A.G. Polnarev, *Primordial black hole formation in the radiative era: Investigation of the critical nature of the collapse*, *Class. Quant. Grav.* **26** (2009) 235001 [0811.1452].
- [117] I. Musco and J.C. Miller, *Primordial black hole formation in the early universe: critical behaviour and self-similarity*, *Class. Quant. Grav.* **30** (2013) 145009 [1201.2379].
- [118] S. Young, C.T. Byrnes and M. Sasaki, *Calculating the mass fraction of primordial black holes*, *JCAP* **07** (2014) 045 [1405.7023].
- [119] K. Ando, K. Inomata and M. Kawasaki, *Primordial black holes and uncertainties in the choice of the window function*, *Phys. Rev. D* **97** (2018) 103528 [1802.06393].
- [120] J.-P. Li, S. Wang, Z.-C. Zhao and K. Kohri, *Primordial non-Gaussianity f_{NL} and anisotropies in scalar-induced gravitational waves*, *JCAP* **10** (2023) 056 [2305.19950].
- [121] J.-P. Li, S. Wang, Z.-C. Zhao and K. Kohri, *Complete analysis of the background and anisotropies of scalar-induced gravitational waves: primordial non-Gaussianity f_{NL} and g_{NL} considered*, *JCAP* **06** (2024) 039 [2309.07792].
- [122] Z. Chang, Y.-T. Kuang, D. Wu, J.-Z. Zhou and Q.-H. Zhu, *New constraints on primordial non-Gaussianity from missing two-loop contributions of scalar induced gravitational waves*, *Phys. Rev. D* **109** (2024) L041303 [2311.05102].
- [123] V. De Luca, A. Kehagias and A. Riotto, *How well do we know the primordial black hole abundance: The crucial role of nonlinearities when approaching the horizon*, *Phys. Rev. D* **108** (2023) 063531 [2307.13633].
- [124] A.J. Iovino, S. Matarrese, G. Perna, A. Ricciardone and A. Riotto, *How well do we know the scalar-induced gravitational waves?*, *Phys. Lett. B* **872** (2026) 140039 [2412.06764].
- [125] G. Domènech, S. Pi, A. Wang and J. Wang, *Induced gravitational wave interpretation of PTA data: a complete study for general equation of state*, *JCAP* **08** (2024) 054 [2402.18965].
- [126] L. Liu, Z.-C. Chen and Q.-G. Huang, *Probing the equation of state of the early Universe with pulsar timing arrays*, *JCAP* **11** (2023) 071 [2307.14911].
- [127] S. Pi, *Non-Gaussianities and Primordial Black Holes*, 2404.06151.
- [128] G. Domènech and S. Pi, *NANOGrav hints on planet-mass primordial black holes*, *Sci. China Phys. Mech. Astron.* **65** (2022) 230411 [2010.03976].
- [129] V. Vaskonen and H. Veermäe, *Lower bound on the primordial black hole merger rate*, *Phys. Rev. D* **101** (2020) 043015 [1908.09752].
- [130] V. De Luca, G. Franciolini, P. Pani and A. Riotto, *Constraints on Primordial Black Holes: the Importance of Accretion*, *Phys. Rev. D* **102** (2020) 043505 [2003.12589].
- [131] Y. Ali-Haïmoud and M. Kamionkowski, *Cosmic microwave background limits on accreting primordial black holes*, *Phys. Rev. D* **95** (2017) 043534 [1612.05644].